Synthesis and *in vivo* evaluation of a scaffold containing wollastonite/β-TCP for bone repair in a rabbit tibial defect model

Willams Teles Barbosa [1], Katilayne Vieira of Almeida [1], Gabriel Goetten de Lima [2-3], Miguel A. Rodriguez [4], Marcos V. Lia Fook [1], Raul García-Carrodeguas [5], Monique Silva Avelino [6], Francisco Alipio de Sousa Segundo [6], Marcelo Jorge Cavalcanti de Sá [3,6]*

[1] Certbio, Universidade Federal de Campina Grande (UFCG), Campina Grande-PB, Brazil.

[2] Programa de Pós-Graduação em Engenharia e Ciência dos Materiais - PIPE, Universidade Federal do Paraná, Curitiba, PR, Brazil.

[3] Materials Research Institute, Athlone Institute of Technology, Athlone, Ireland.

[4] Institute of Ceramics and Glass (CSIC), Madri, Espanha.

[5] Noricum S.L., Madrid, Spain.

[6] Programa de Pós-Graduação em Medicina Veterinária (PPGMV), Universidade Federal de Campina Grande (UFCG), Campina Grande PB, Brasil.

E-mail: mjcdesa@gmail.com. * Corresponding author.

Abstract

Scaffolds are models designed to aid the interaction between cells and extracellular bone matrix, providing structural support for newly formed bone tissue. In this work, wollastonite with β-tcp porous ceramic scaffolds were developed by the polymer sponge replication. Their microstructure, cell viability and bioactivity were tested. In vivo was performed to evaluate the use of a calcium silicate-based implant in the repair of rabbit tibias. Holes were made in the both proximal and distal tibial metaphysis of each animal and filled with calcium silicate-based implant, and in the left tibia, no implant were used, serving as control group. Animals underwent euthanasia after 30 and 60 days of study. The animals were submitted to clinical-radiographic evaluations and its histology were analyzed by optical and scanning electron microscope. The studied calcium silicate implant provided biocompatibility and promoted bone formation, stimulating the process of bone repair in rabbits, features observed by gradual radiopacity shown in the radiographic evaluations.

Keywords: bioceramics; calcium phosphate; calcium silicate; bone regeneration

1. Introduction

Bone is an essential organ that plays fundamental roles in human physiology, including protection, movement and support of other organs, blood production, storage of minerals and homeostasis, regulation of pH in the blood and many others. The importance of bone becomes clear in the case of diseases such as osteogenesis imperfecta, osteoarthritis, osteomyelitis and osteoporosis in which the bone does not function properly. These diseases, along with traumatic injuries, orthopedic surgeries and primary tumor resection lead to or induce bone defects or voids. The clinical and economic impact of treatments for bone defects is striking [1,2]; therefore, research alternatives to reverse bone defects and regenerate bone damage is of great importance [3].

One of the bone regeneration materials currently available in the market is allografts; however, they suffer from immune rejection, reduced bioactivity and risk of transmitting pathogens. Although largely used as biomedical materials, metallic implants have limited osseointegration and use; therefore, there is a need to find other alternatives for bone tissue engineering [3,4].

Between the important characteristics for implants used as bone regeneration applications lists the needs of appropriate mechanical properties; adequate chemical composition and degradation; nontoxic and biodegradability with simple and effective manufacturing technology [5]. Currently, the need to support the load bearing by normal day-to-day use of implant coupled with the idea a biodegradability with a rate similar to the deposition of new bone have been gathering many attractive research focus [6,7]. In addition to providing mechanical support to cell colonization, the new framework should stimulate the migration, adhesion and differentiation of osteoprogenitor cells, as well as encourage angiogenesis [8].

Most commercial calcium phosphates bioceramic are composed of Hydroxyapatite (HAp, $CA_{10}(PO_4)_6(OH)_2$), tricalcium β-phosphate (β-TCP, $β-Ca_3(PO_4)_2$), or a mixture of the two, named biphasic calcium phosphate (BCP) [9–11]. Calcium phosphate-based materials have attracted considerable interest for orthopedic applications due to its useful characteristics such as good biocompatibility between the ceramic and the extracellular matrix, fast proliferation compared to non-phosphate materials and proliferation of a healthy tissue growth directly on its surface [12]. As a specific group

from calcium phosphate ceramics, tricalcium phosphate (TCP), used as bioceramic implants, have good rates of bioabsorption couple with its good cell-ceramic interaction. The chemical composition of the $CA_3(PO_4)_2$ and the Ca/P ratio of 1.5 is similar to bone ratio and even though calcium phosphate is more closely related to bone crystallography, the rate of reabsorption of TCP is about 3 to 12 times faster than common ceramics [13].

Besides common calcium phosphate-based ceramics, researchers have been trying to use wollastonite from various sources and synthesis as a biomaterial [14–16]. This calcium silicate reacts fast in simulated body fluid [17] and the response in vivo demonstrates that osteoblasts migrate to the surface of wollastonite and colonized the surface at the contact areas with the cortical regions and also bone marrow [18,19].

One of the easiest methods to produce scaffolds from ceramic powders is the polymeric sponge replica; which is a simple and inexpensive method, by impregnating into the polymeric sponge a ceramic suspension and subsequent burning of the polymer prior to sintering which has a prominent attention due to its potential to form uniform dispersion of its ceramic powders within the polymer supports with high porosity and interconnected pores since it is possible to obtain a scaffold that follows the porosity distribution and size of the sponge [20].

Therefore, in this work we developed a porous three-dimensional structure - *scaffolds* - with mixed composition of 40% beta tricalcium phosphate (β-TCP) and 60% pseudowollastonite (PSCs) obtaining the eutectic composition of this material after sintering [21]. *Scaffolds* were obtained using the polymer sponge replica technique. By the use of wollastonite and tricalcium phosphate as a ceramic suspension; this material can provide a controlled release of calcium, silicon and phosphorus in order to improve osseointegration as it was tested in vivo in a rabbit tibial defect model.

2.   Materials and Methods.

2.1 Materials

Natural Wollastonite (W) (M400, Nycon); Tricalcium β-phosphate (β-TCP) previously synthesized in a laboratory from hydroxyapatite - HAp (Labsynth, Brazil); dispersant based on polyacrylate (Dolapix PCN Zschimmer-Schwarz) and polyvinyl alcohol binder (PAF Optapix 35, Zschimmer-Schwarz) were used as raw materials and additives for the preparation of the samples.

2.2 Tricalcium β-phosphate synthesis

β-TCP was synthesized by the HAp neutralization reaction using Orto-phosphoric acid (H_3PO_4, 85%, Labsynth, Brazil) to obtain a Ca/P ratio of 1.5. The suspension was stirred for 30 minutes and dried at 65 ºC for 24 hours and the dry residue was treated at 1000 º C for 15 hours.

2.3 Scaffold synthesis

The composition of 60 (WT.%) of W (wollastonite)-40 (WT.%) of β-TCP corresponds to the composition of eutectic in the $CaO. SiO_2$-$3CaO. P_2O_5$ system. In order to homogenize and decrease its particle size, particles were grinded in isopropyl alcohol with 1 to 2 mm alumina spheres for 4 h following by drying in a oven at 65 ºC for 24 h and deagglomerated. Scaffolds were obtained by the impregnation method using a polyurethane sponge of open pores of 60 ppi (Prosider, S.A.) in the form of an 8 mm diameter and 2 m thick disc. The aqueous suspension was prepared using a solid content of 30% in volume, 0.3% in dispersant volume and 0.5% in ligand volume.

The impregnated sponges were burned according to the following thermal cycle: Heating at 2 º C/min up to 600 º C for the removal of the polymer, 1275 °C at 5 °C/min and permanence for 2 hours for sintering, followed by cooling at 2 º C/min) up to 1000 ºC , finishing with cooling to room temperature at 5 º C/min.

2.4 Microstructure, morphology and particle size

The identification of crystalline phases of the powders and *scaffold* was performed by analysis of X-ray Difration analysis using a Diffractometer D8 bruker (Bruker, Germany) with CuKα radiation (λ = 1.5406 Å), working at 40 KV and 40 MA. For the acquisition, Diffractograms were recorded in step mode at an angle of 2θ between 15-60º, with a step of 0.02° and acquisition time of 4 s. The X'pert HighScore Plus (PANalytical, Netherlands) software was used for qualitative phase analysis.

The morphology of the powders and *scaffolds* was evaluated by scanning electron microscopy (TM 1000, Hitachi, Japan) by backscattering mode.

The powders were characterized by measuring its particle size using the laser scattering method (Mastersizer S, Malvern).

2.5 Bioactivity and cytotoxicity

In vitro bioactivity of the samples was evaluated according to ISO 23317:2012 (Implants for surgery -- In vitro evaluation for apatite-forming ability of implant materials). The test was performed on discs (5 mm height; 10 mm diameter) by incubation in SBF at 36 ± 1 ° C for 14 days. After this period, these samples were removed from the solution, dried and covered by gold, the presence of the apatite layer was verified by SEM.

To evaluate the cell deposition in the scaffolds, the fibroblast cells were cultivated in rpmi-1640 medium in incubators with 5% CO_2 atmosphere at 37 ° C, with controlled humidity. The culture medium was exchanged 2 to 3 times per week. After 7 days, the cavities were washed with buffered saline solution (PBS) and the cells were fixed with 10% formaldehyde solution for 10 minutes. The scaffolds were covered by gold sputtered and prior analysis by the SEM.

2.6 *In vivo* methodology

The research project was evaluated and approved by the Research Ethics Committee of the Federal University of Campina Grande number 031.2017. For *in vivo* evaluations, 12 rabbits, males and females, of the New Zealand lineage with an average weight of 3 kg were used in this study. These animals were maintained in a temperature-regulated environment and housed individually in rabbit cages under the same feeding and management conditions, previously sanitized and suspended from the soil, acclimatized for a seven-day adaptation period prior the experiments.

2.6.1 Anesthetic and surgery procedure

Prior to surgery, the animals were submitted to feeding fasting of 6 h, and water of 3 h; also, the hairs of the pelvic limbs and lumbosacral region were removed. For the anesthetic protocol xylazine at 2% (5 mg/kg) and hydrochloride ketamine at 5% (30 mg/kg), both intramuscularly. The administration of 2% lidocaine (0.3 ml/kg) and tramadol 5% (1 mg/kg) was continued, both by epidural route. Approximately 30 minutes before the surgical procedure, enrofloxacin was administered, 10 mg/kg, intravenously.

A 2-cm-long incision was made at the proximal and distal cranium-medial margin of each tibia, followed by a subcutaneous and muscular tissue divulsion until the periosteum was exposed. Two orifices (one proximal and one distal) of 2.0 mm diameter were performed with the aid of an orthopedic drill under constant irrigation of

0.9% NaCl solution in the proximal and distal metaphysis of the bone. In the right limb was implanted the calcium silicate in both created holes and in the left limb, used as a control, the bone holes were not filled with any implants. Afterwards, the muscle was synthesized with a suture of 3-0 polyglactin 910 in "x" pattern also used for reduction of the subcutaneous dead space in an intradermal pattern, and dermorrhaphy with standard nylon 3-0 Wolf.

During the postoperative period, the animals received tramadol (10 mg/kg) intramuscularly, every 24 hours for 3 days, and daily cleaning of the surgical wound with 0.9% NaCl solution for 10 days, and then the removal of the surgical sutures was performed.

2.7 Postoperative evaluation

2.7.1 Clinical evaluation

A clinical-orthopedic evaluation was performed, observing the presence or absence of claudication, edema, pain sensitivity, dehiscence and surgical wound infection, during the first 10 days after the surgical procedure.

2.7.2 Radiographic evaluation

For radiographic analysis, radiographs of both tibias were performed in the mediolateral and craniocaudal projections, immediately after surgery, at 30 and 60 days postoperatively. The radiographic technique was standardized (45Kv, 100mA and 0, 03s), and the radiographs were analyzed subjectively, considering characteristics and intensity of reactions of the osseous bone.

2.7.3 Euthanasia

The animals were euthanized after 30 days (group 1) or 60 days (Group 2) of the surgical procedure for histopathologic evaluation. The euthanasia protocol adopted consisted of administration of the combination of 2% xylazine (5 mg/kg) and ketamine at 5% (40 mg/kg), both intramuscularly. After 15 minutes, 1% propofol (5 mg/kg) was administered, followed by potassium chloride 19.1% (1 ml/kg), both intravenously.

2.7.4 Processing of *in vivo* samples

Bone samples containing the orifices or calcium silicate implants were collected and fixed in 10% formalin. Each recipient was identified with the number of the animal and the group to which it belonged. After the fixation period (three days), samples were decalcified in 10% nitric acid solution for a period of five days. Then, the pieces were routinely processed and included in paraffin. The slices were made with a 5 mm thickness, semi-serial 1in Manual Rotary microtome Ek Micro1 (Eikonal do Brasil, São Paulo, SP, Brazil) with a thickness of 5 mm, semi-serial of 1/5, and stained by the technique of hematoxylin of harris and eosin alcoholic (H/E).

2.7.5 Morphometric evaluation

The slides obtained at 30 and 60 postoperative days were evaluated by the morphometry process for quantification of the bone tissue repair, comparing the groups to each other in each moment, through the MvImage program version 3.1®. To perform this analysis digitization of the images that comprised the bone/implant and bone/defect interface were made. Sequenced images of each slides analyzed were obtained to quantify all the newly formed tissue in all areas of the bone gap. The mean values obtained for each group were obtained and submitted to statistical analysis.

2.7.6 Statical analysis

For the comparison of the groups for morphometric evaluation, the Kruskal-Wallis test was conducted with multiple comparisons by the Nemenyi test. The level of significance adopted in all analyses was 5% and the software BioEstat 5.03 was used.

2.7.7 Histology analysis by optical microscopy and scanning electron microscopy (SEM)

The processed samples were then evaluated by optical microscopy through comparative descriptive analysis. These samples were also evaluated using the scanning microscopy (SEM) technique.

3. Results and discussion

3.1 Powder microstructure

The results of the XRD identification of the crystalline phases present in the powders are shown in Figure 1. The presence of a single crystalline phase was identified in

relation to β-TCP with a rhombohedral structure and R-3c space group in accordance with JCPS 00-009-0169. No peaks corresponding to the HAp phase were observed, indicating complete phase transition; also, it was possible to identify the presence of a single crystalline phase referring to Parawollastonite with monoclinic crystalline system and space group P21/A in accordance with JCPDS 00-043-1460.
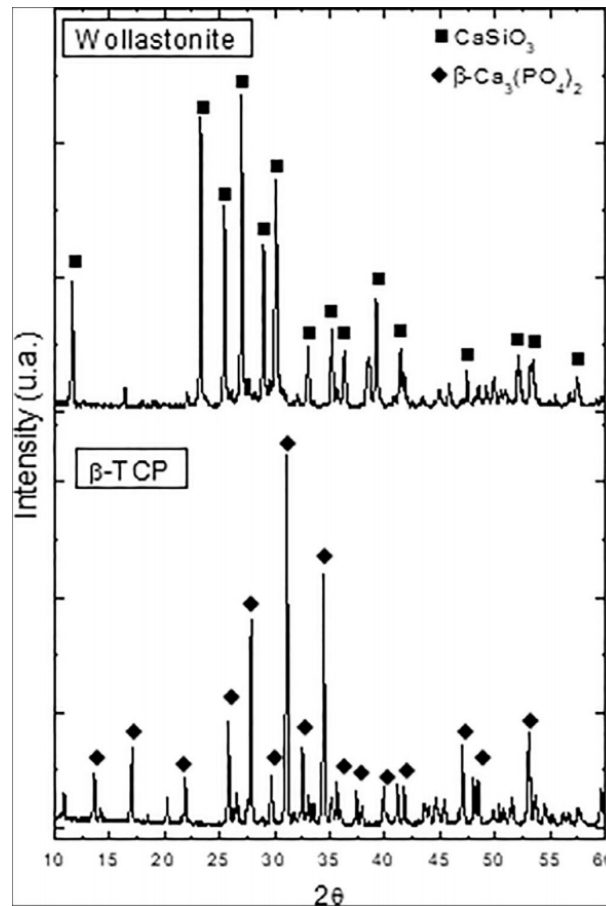

FIGURE 1. X-ray diffractogram of the raw powders—wollastonite and β-TCP. β-TCP, tricalcium β-phosphate

3.2 Powder Morphology

The characterization of the powders through the morphological analysis using a scanning electron microscope (Figure 2) exhibits that the shape of both materials is quite different. Wollastonite has an acicular shape with large platelet-like aggregates (Fig. 2 (a)), with an average particle size (D50) of 4.6 µm. The β-TCP powders present smaller sizes compared to Wollastonite, with the formation of some spherical agglomerates (Fig. 2 (b)), and an average particle size (D50) of 3.7 µm.

Therefore, this is the reason these materials were grinded prior formation of the scaffolds; to obtain more uniform particles for better process control. After grinding by

friction, the average particle size (D50) for wollastonite powder was 2.3 µm and 1.6µm for β-TCP powder. These grinded powders presented acceptable particle sizes for the production of the scaffolds.
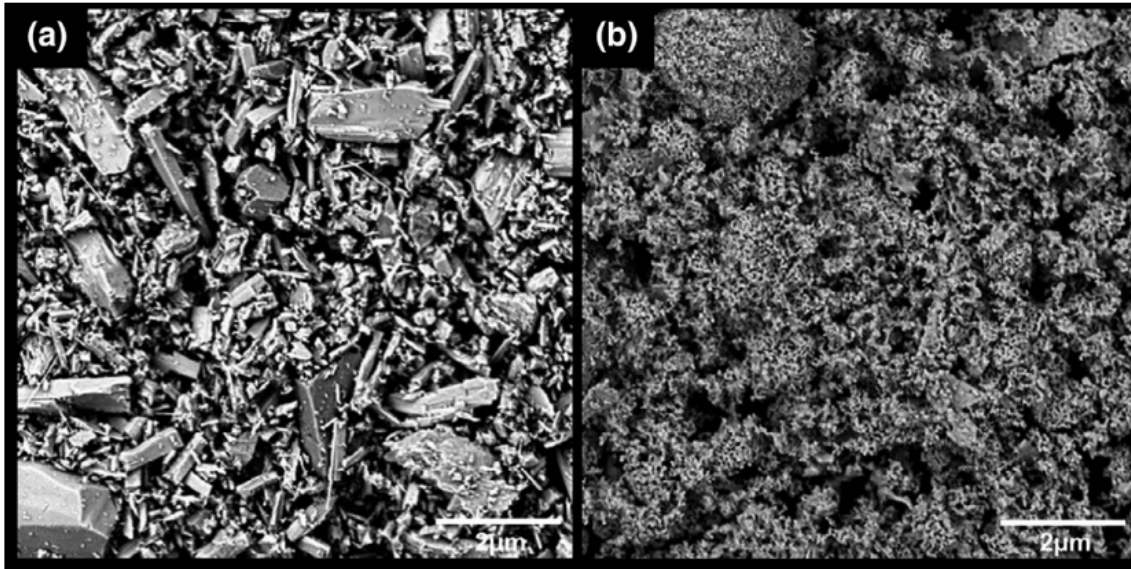

FIGURE 2. SEM micrographs of raw powders wollastonite (a) and β-TCP (b). β-TCP, tricalcium β-phosphate

3.3 Scaffold morphology

Scaffold synthesized at 1275 ° C follows the structure referring to the sponge used as a mold (Figure 3 (a)). From the SEM image (Figure 3 (b)) it is possible to observe relatively dense macropores and filaments with the ceramic phase, with no cracks in their structure.
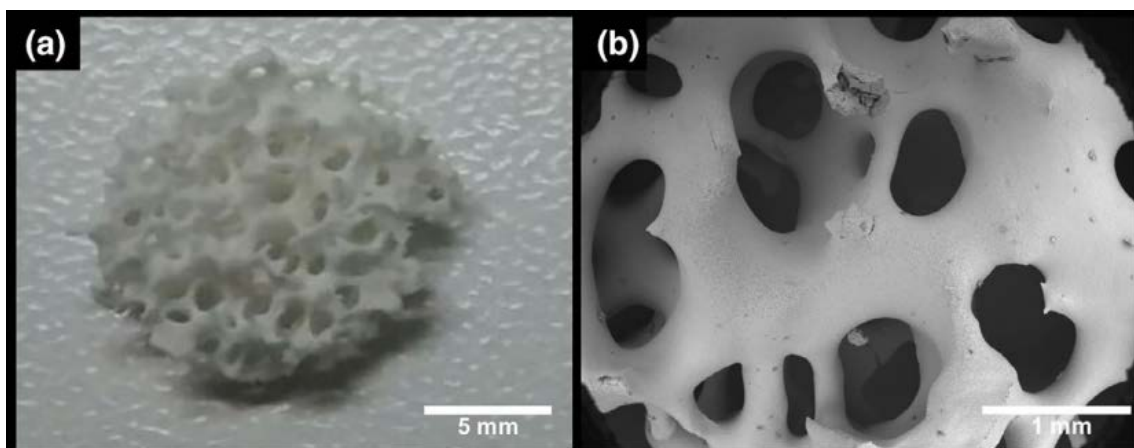

FIGURE 3. (a) Macroscopic evaluation of the scaffold and (b) SEM of the scaffold surface.

The strength of the material is sufficient for handling without risk of rupture. The main function of this scaffold is to act temporarily as a support, facilitating and guiding cell growth until complete tissue regeneration.

The porosity of this scaffold has, as main characteristic, the interconnectivity responsible for the maintenance and growth of the bone tissue, for nutrient transport and drainage of interstitial liquids. The tissue regeneration is related to the pore size of the scaffolds [22]. The minimum size required for bone regeneration is 100 - 350 μm. Pores smaller than 75 - 100 μm result in the growth of non-mineralized osteoid tissue. In addition, pores smaller than 5 μm allows neovascularization and 5-15 μm fibroblast growth [23,24].

3.4 Scaffold microstructure

The XRD of scaffold powder (Figure 4) exhibited the peaks corresponding to the crystalline phase of pseudowollastonite ($Ca_3(Si_3O_9)$) with C-1 space group and anorthic crystal system in accordance with JCPDS 01-074-0874. It was identified the presence of the β-TCP (β-$Ca_3(PO_4)_2$) phase with rhombohedral crystalline system, space group R-3c, in accordance with JCPDS 00-009-0169.
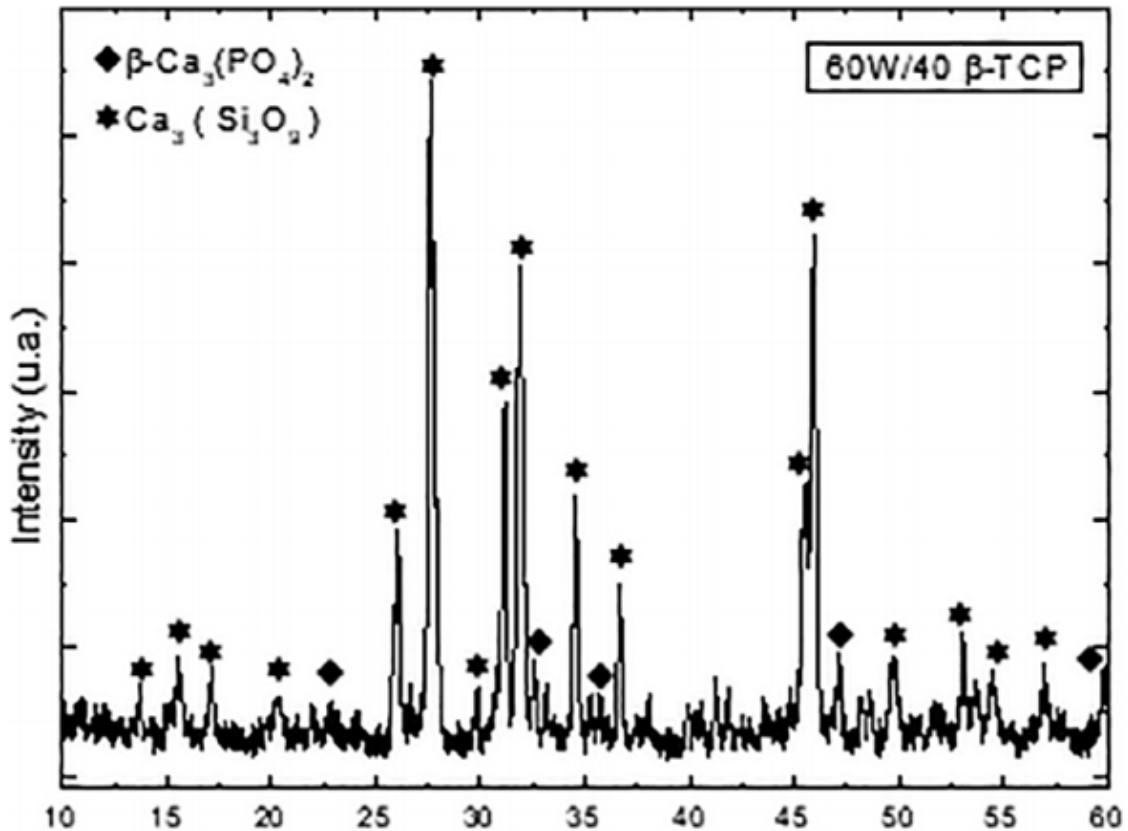

FIGURE 4. Scaffold powder diffractogram.

3.5 Scaffold bioactivity and cellular response

Figure 5 (a) exhibits SEM micrographs of scaffold after immersion in SBF solution for 14 days, it is possible to observe the deposition of a new layer, with the formation of globules with different sizes along the surface. This profile is typical morphology of apatite layer formation as shown in ceramics and different materials [25,26].
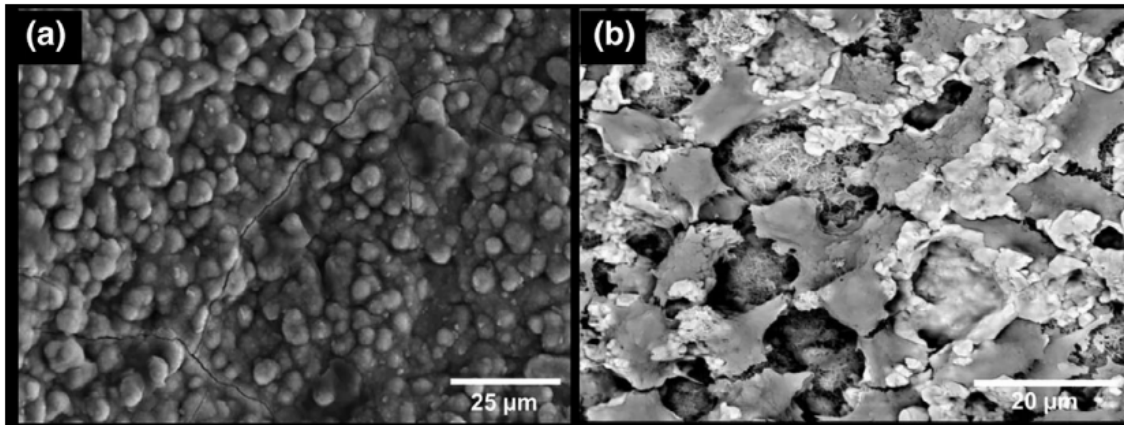

FIGURE 5. SEM micrographs of the scaffold surfaces after immersion in SBF for 14 days (a) and cell adhesion for peer review for 7 days (b).

The mechanism of apatite formation from this structure is that first CA^{2+} ions of the crystalline lattice are replaced by existing H^+ ions in the medium (SBF) and as a result a layer of hydrated silica and amorphous is formed. Due to the incorporation of $H+$ into hydrated silica, the pH in the solid-liquid interface increases to approximately 10.5, which leads to partial dissolution of amorphous hydrated silica and apatite precipitation on the surface of the material, promoting the adhesion of Cells [27,28]

The micrographs exhibits that after 7 days of the cell adhesion assay (Figure 5 (b)) the surface of the scaffolds had adhered cells along their structure, but also exhibited extensions between adjacent cells.

Cellular deposition shows steps from the first cellular deposition, such as spreading processes and cellular interdigitations, the coated samples showed invagination to the scaffold confirming cellular preference by the scaffold surface and the osteoconductive character of wollastonite.

3.6.1 Postoperative observation from *in vivo* analysis

All animals evaluated in this study did not present, during the clinical-orthopedic evaluation, any clinical sings of lameness, edema, pain, sensitivity, dehiscence of points or infection. A Few hours after the surgical procedure all the animals supported the limb

and wandered without claudication [29,30]. The functional return of the limb is related to the precise surgical procedure, adequate analgesic management and biocompatibility of the implant used. Depending on the surface chemistry of this material and cell interaction, the postoperative period of the animal may present claudication for the animals for a period of up to seven days and there have been methods to avoid bacterial contaminations [31]. Therefore, it is possible to induce that the implant already presented good biocompatibility.

3.6.2 Radiographs of the scaffolds after implantation

In Radiographs performed immediately after surgery, it was possible to visualize radiolucent halos (Figure 6), which gradually decreased, and after 60 days they were already similar to that of bone tissue; revealing adequate absorption and incorporation of the implants into the bone structure.
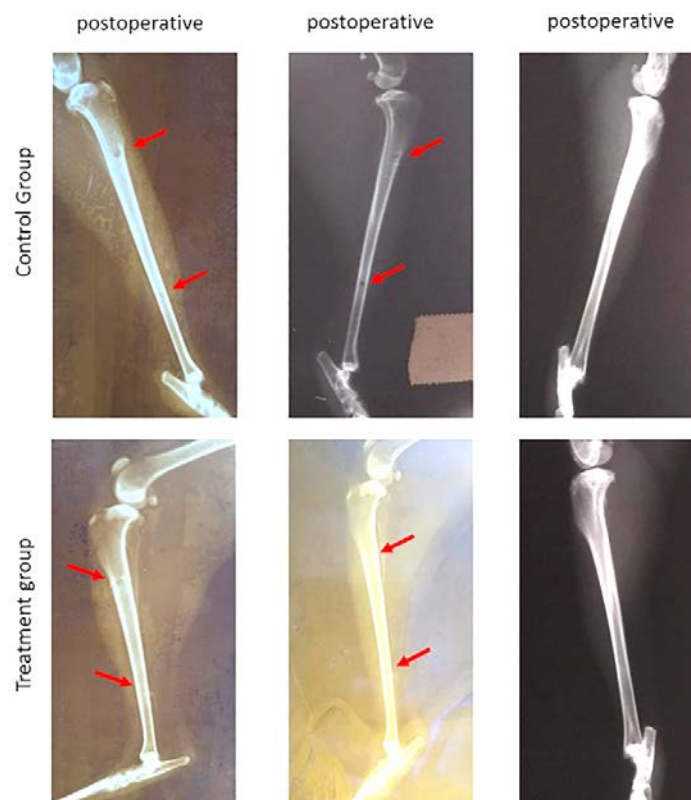

FIGURE 6. Radiography of rabbits' tibia submitted to calcium silicate implant. (a) Immediate postoperative—observe the implant areas in the distal and proximal metaphyseal region. (b) After 30 days—a radiolucent area was observed involving the cortex in the proximal and distal area at the implanted site in both groups. (c) After 60 days—absence of radiolucent halo at the implant placement sites, soft tissue radiopacity and preserved cortical in both groups.

This fact was favored by the similar chemical structure of the implants to those of the bone tissue, allowing a gradual biodegradation.

In the case of 30 days from control group, the bone halo observed immediately after surgery still persists and its decrease could be observed only after 60 days. For the groups containing the implant, radiographic evaluation after 30 days revealed that one of the animals presented a discrete periosteal reaction with osteocyte proliferation adjacent to the implant-containing hole in the right tibia metaphysis. In the other five animals from the same group a radiolucent area was observed involving the cortical at the implanted site, with absence of periosteal reaction and signs of inflammatory process. These evidences the process of biodegradation of the implant and suggests adequate biocompatibility of the material. The use of bioceramics tends to promote a more discreet bone neoformation, which may explain the discrete periosteal reaction observed in a single animal in the present study [32].

After 60 days, the absence of a radiolucent halo at implant preserved sites and preserved cortices were observed, indicating an advanced phase on the implant absorption and suggesting that calcium silicate exhibits a relatively faster resorption rate when compared to other bioceramics.

3.6.3 Histology analysis

A significant difference ($p < 0.05$) was observed in the amount of neoformed tissue between groups at both time intervals (Table 1). This ceramic supplies the necessary materials to help accelerate the bone repair process. Similar results are found with the use of ceramics isolated or associated with other products [33].

Table 1. Mean and standard deviation of the area in μm^2 obtained through histomorphometry of the newly formed tissue at the bone/implant (treatment group) and bone defect (control group) interface in the tibial shaft of rabbits.

	30 days postoperative	60 days postoperative
Treatment group	39.542,12 ± 13.641,78a	73.132,43 ± 15.942,10a
Control group	20.726,51 ± 14.934,32b	32.657,85 ± 12.874,73b

Means followed by diverse letters on the same column presented statistical difference ($p < 0.05$) by the Kruskal-Wallis test.

Bioceramics have similar composition to bone matrix, because this characteristic these implants may contribute significantly to osteoconduction, this effect has been shown by several authors [11,17], which was also perceived in the present study.

The production of bioceramic implants that allow its association seems to be the most efficient method of its use, its longer time of biodegradation and its performance in a more specific step of the bone repair compensated by the properties of other polymers, these associations have been showing good results [34].

3.7.1 Optical Microscope analysis

Histology analysis from optical microscope exhibits (Figure 7) a discrete reorganization of compact bone tissue with the control group (Figure 7 a-b) and a discrete periosteal reaction in the holes and with implants at 30 days (Figure 7 c-d). For 60 days (Fig. 7 d-e), there was a focal area of bone remodeling and bone matrix proliferation around the implanted material.
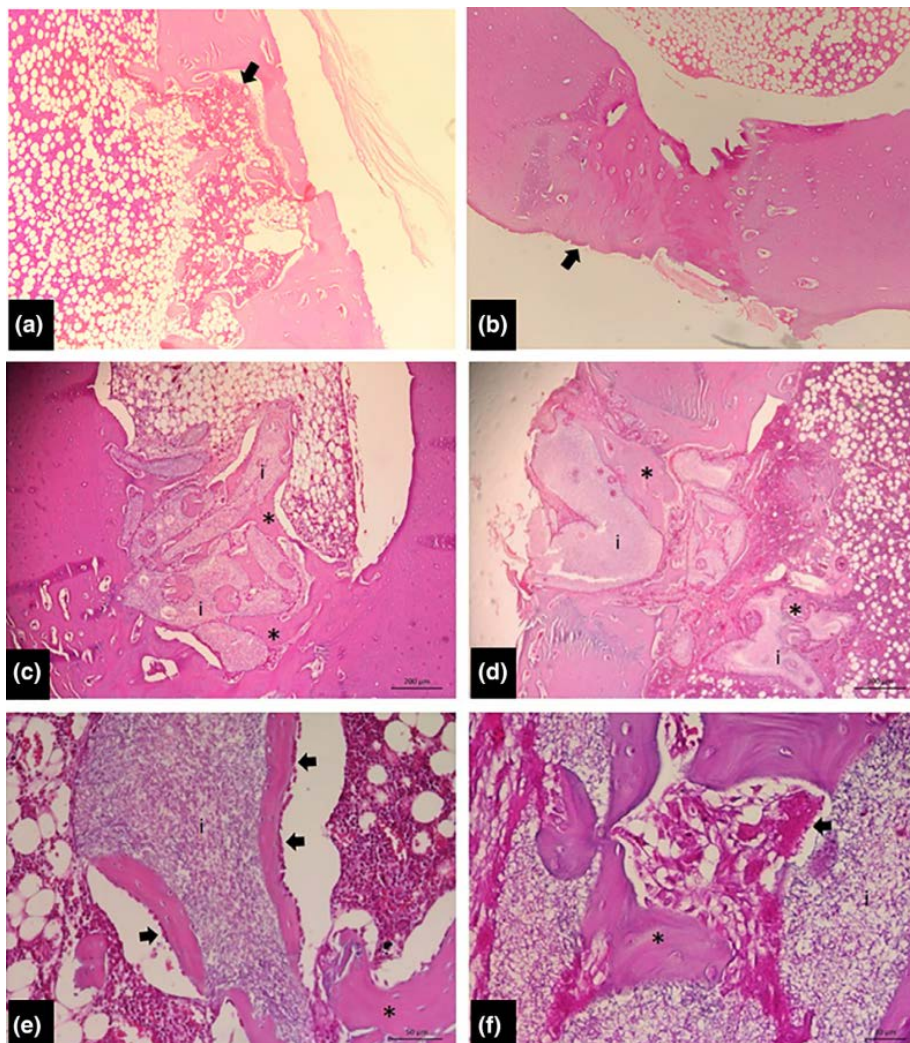
FIGURE 7. Photomicrography histology analysis. (a) Control group at 30 days after surgery in rabbit tibia submitted to osteotomy, the bone remodeling area of compact bone is observed with presence of discrete proliferation of bone matrix (arrow). (b) At 60 days after surgery; few osteoblasts surrounding the neoformed bone tissue (arrow). (c) At 30 days after surgery in rabbit tibia submitted to calcium silicate implantation; the bone remodeling area of compact bone is observed with presence of moderate material fibrillar, irregular and eosinophilic; detailed region of the calcium silicate implant (i) and proliferation of bone matrix (*). (d) Specific region of the discontinuity area of the compact bone associated with fibrillar, irregular and eosinophilic material (implant) (i) and proliferation of bone matrix (*). (e) At 60 days after surgery; multiple osteoblasts surrounding the neoformed bone tissue (arrows), in addition to the calcium silicate implant (i) and proliferated bone matrix (*). (f) Specific region where the presence of multiple osteoclasts (arrow) is observed amid proliferation of bone matrix (*).

Around the implant, bone tissue formed in a disorganized way, reaching up the medullary area already at 30 days, this is further intensified at 60 days. It is known that calcium-based ceramics promote a direct interaction with the bone tissue, without interposition of the fibrous tissue [35]. In addition, calcium present in ceramics has a complex surface capable of favoring platelet activation, initiating cellular phenomena that culminate in bone neoformation [36].

No inflammatory reaction or necrosis was observed during histopathological analysis, confirming the low cytotoxicity and high biocompatibility of the implant.

3.7.2 Scanning Electron Microscope analysis

The implants were covered by bone tissue and there was no inflammatory reaction (Figure 8). It is evidenced that the coloration varied from whiter regions to dark gray, close to black. Near the implant region, there was a light gray structure, which may be associated with the presence of young bone tissue. In addition, there was a decrease in the amount of biomaterial in the region at the bone-implant interface, indicating reconstruction of the damaged bone tissue. Similar results were obtained by other authors for SEM analysis on absorption of cements [37].

The bioactivity was present from the first day over the period of 14 days, it was possible to observe steps of precipitation, nucleation and deposition of calcium phosphate on the

surface of these scaffolds, in addition, the most evident layer thickness in the scaffold 80% W + 20% β-TCP shows overlapping layers, indicating high bioactivity of this composition.
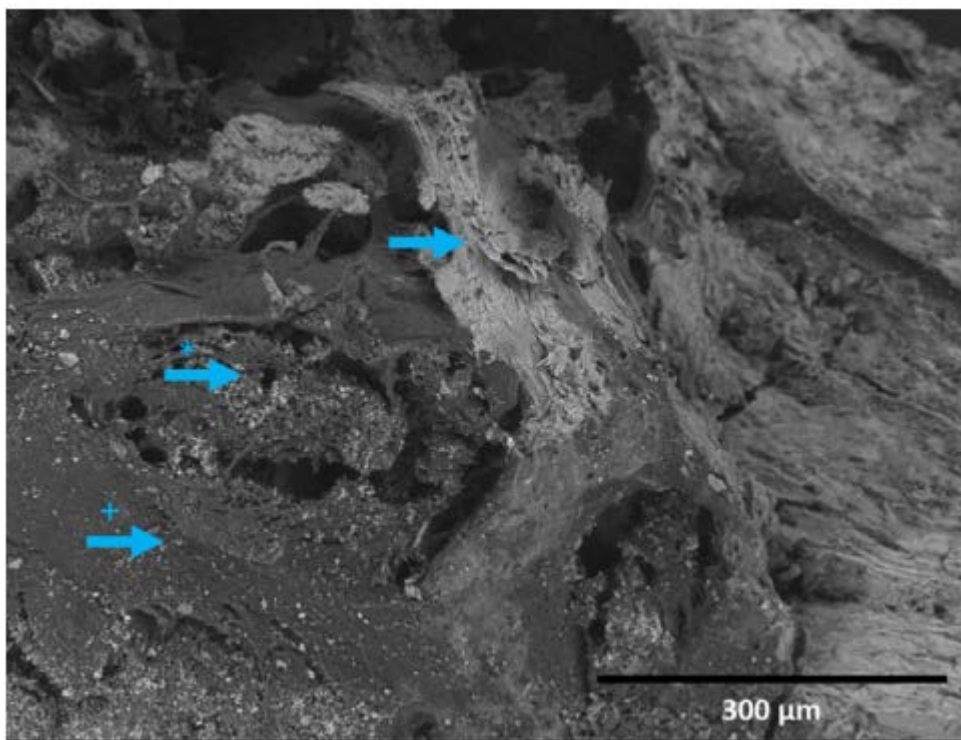

FIGURE 8. Scanning electron microscopy image after 60 days of calcium silicate implant in rabbit tibia. Variation on scale of gray indicates that lighter gray area ($\rightarrow$ sign) shows the old bone tissue, and the darker gray area ($\rightarrow$+ sign) shows newly formed bone surrounding the implant ($\rightarrow$* sign). Increase of 300x.

Finally, cellular deposition shows steps from the first cellular deposition, such as spreading processes and cell interdigitations, the coated samples showed cell invaginations confirming cellular preference by the scaffold surface, confirming the osteoconductive character of Wollastonite.

Conclusion

The polymeric sponge replica method adopted for scaffolds processing in this work can be considered as effective and reproducible, its porous structure is excellent for permeation for cells, nutrients and residues. The formulated scaffolds are promising, as it has a bioactive and osteoconductive character proven by the adhesion of cells to the surface of the material. It was also verified that the calcium silicate when implanted in tibia of rabbits had an earlier stimulation in the process of bone repair, besides presenting characteristics of biocompatibility and no cytotoxicity.

References

[1] Porter JR, Ruckh TT, Popat KC. Bone tissue engineering: A review in bone biomimetics and drug delivery strategies. Biotechnol Prog 2009;25:1539–60. doi:10.1002/btpr.246.

[2] Farokhi M, Mottaghitalab F, Shokrgozar MA, Ou K-L, Mao C, Hosseinkhani H. Importance of dual delivery systems for bone tissue engineering. J Control Release 2016;225:152–69. doi:10.1016/J.JCONREL.2016.01.033.

[3] Zhang D, Wu X, Chen J, Lin K. The development of collagen based composite scaffolds for bone regeneration. Bioact Mater 2018;3:129–38. doi:10.1016/j.bioactmat.2017.08.004.

[4] Agarwal R, García AJ. Biomaterial strategies for engineering implants for enhanced osseointegration and bone repair. Adv Drug Deliv Rev 2015;94:53–62. doi:10.1016/j.addr.2015.03.013.

[5] Chen F-M, Wu L-A, Zhang M, Zhang R, Sun H-H. Homing of endogenous stem/progenitor cells for in situ tissue regeneration: Promises, strategies, and translational perspectives. Biomaterials 2011;32:3189–209. doi:10.1016/J.BIOMATERIALS.2010.12.032.

[6] Denry I, Goudouri O-M, Fredericks DC, Akkouch A, Acevedo MR, Holloway JA. Strontium-releasing fluorapatite glass-ceramic scaffolds: Structural characterization and in vivo performance. Acta Biomater 2018;75:463–71.

[7] Dawson JI, Kanczler J, Tare R, Kassem M, Oreffo ROC. Concise review: bridging the gap: bone regeneration using skeletal stem cell-based strategies - where are we now? Stem Cells 2014;32:35–44. doi:10.1002/stem.1559.

[8] Bose S, Roy M, Bandyopadhyay A. Recent advances in bone tissue engineering scaffolds. Trends Biotechnol 2012;30:546–54. doi:10.1016/j.tibtech.2012.07.005.

[9] De Aza PN, De Aza AH, De Aza S. Crystalline bioceramic materials. Bol La Soc Española Ceram y Vidr 2005;44:135–45.

[10] Legeros RZ, Lin S, Rohanizadeh R, Mijares D, Legeros JP. Biphasic calcium phosphate bioceramics: Preparation, properties and applications. J Mater Sci Mater Med 2003;14:201–9. doi:10.1023/A:1022872421333.

[11] Dorozhkin S. Bioceramics of calcium orthophosphates. Biomaterials 2010;31:1465–85. doi:10.1016/j.biomaterials.2009.11.050.

[12] Zhou C, Ye X, Fan Y, Ma L, Tan Y, Qing F, et al. Biomimetic fabrication of a three-level hierarchical calcium phosphate/collagen/hydroxyapatite scaffold for bone tissue engineering. Biofabrication 2014;6:035013. doi:10.1088/1758-5082/6/3/035013.

[13] Shiratori K, Matsuzaka K, Koike Y, Murakami S, Shimono M, Inoue T. Bone formation in beta-tricalcium phosphate-filled bone defects of the rat femur: morphometric analysis and expression of bone related protein mRNA. Biomed Res 2005;26:51–9. doi:10.2220/biomedres.26.51.

[14] Palakurthy S, K. VGR, Samudrala RK, P. AA. In vitro bioactivity and

degradation behaviour of β-wollastonite derived from natural waste. Mater Sci Eng C 2019;98:109–17. doi:https://doi.org/10.1016/j.msec.2018.12.101.

[15] Fiocco L, Agnoli S, Pedron D, Secco M, Tamburini S, Ferroni L, et al. Wollastonite-diopside-carbon composite foams from a silicone resin and inorganic fillers. Ceram Int 2018;44:931–7. doi:https://doi.org/10.1016/j.ceramint.2017.10.025.

[16] de Lima GG, Traon F, Moal E, Canillas M, Rodriguez MA, McCarthy HO, et al. Composite cryogels for dual drug delivery and enhanced mechanical properties. Polym Compos 2018;39:E210–20. doi:10.1002/pc.24450.

[17] Núñez-Rodríguez LA, Encinas-Romero MA, Gómez-Álvarez A, Valenzuela-García JL, Tiburcio-Munive GC. Evaluation of Bioactive Properties of α and β Wollastonite Bioceramics Soaked in a Simulated Body Fluid. J Biomater Nanobiotechnol 2018;09:263–76. doi:10.4236/jbnb.2018.93015.

[18] de Aza PN, Luklinska ZB, Martinez A, Anseau MR, Guitian F. Morphological and structural study of pseudowollastonite implants in bone. J Microsc 2000;197:60–7.

[19] Qian G, Fan P, He F, Ye J. Novel Strategy to Accelerate Bone Regeneration of Calcium Phosphate Cement by Incorporating 3D Plotted Poly(lactic- co -glycolic acid) Network and Bioactive Wollastonite. Adv Healthc Mater 2019;8:1801325. doi:10.1002/adhm.201801325.

[20] Wang C, Chen H, Zhu X, Xiao Z, Zhang K, Zhang X. An improved polymeric sponge replication method for biomedical porous titanium scaffolds. Mater Sci Eng C 2017;70:1192–9. doi:https://doi.org/10.1016/j.msec.2016.03.037.

[21] De Aza PN, Guitián F, De Aza S. Phase Diagram of Wollastonite-Tricalcium Phosphate. J Am Ceram Soc 1995;78 (6):1653–6.

[22] Hollister SJ. Porous scaffold design for tissue engineering. Nat Mater 2005;4:518.

[23] Karageorgiou V, Kaplan D. Porosity of 3D biomaterial scaffolds and osteogenesis. Biomaterials 2005;26:5474–91. doi:10.1016/j.biomaterials.2005.02.002.

[24] Whang K, Tsai DC, Nam EK, Aitken M, Sprague SM, Patel PK, et al. Ectopic bone formation via rhBMP-2 delivery from porous bioabsorbable polymer scaffolds. J Biomed Mater Res An Off J Soc Biomater Japanese Soc Biomater Aust Soc Biomater 1998;42:491–9.

[25] de Lima GG, de Souza GB, Lepienski CM, Kuromoto NK. Mechanical properties of anodic titanium films containing ions of Ca and P submitted to heat and hydrothermal treatment. J Mech Behav Biomed Mater 2016;64:18–30. doi:10.1016/j.jmbbm.2016.07.019.

[26] Liu X, Ding C, Chu PK. Mechanism of apatite formation on wollastonite coatings in simulated body fluids. Biomaterials 2004;25:1755–61. doi:10.1016/j.biomaterials.2003.08.024.

[27] De Aza PN, Guitian F, Merlos A, Lora-Tamayo E, De Aza S. Bioceramics - simulated body fluid interfaces: PH and its influence of hydroxyapatite

formation. J Mater Sci Mater Med 1996;7:399–402. doi:10.1007/BF00122007.

[28] Wu C, Xiao Y. Article Commentary: Evaluation of the In Vitro Bioactivity of Bioceramics. Bone Tissue Regen Insights 2009;2:BTRI.S3188. doi:10.4137/BTRI.S3188.

[29] Ferreira ML, Silva PC, Alvarez Silva LH, Bonfim DC, Conilho Macedo Müller LC, Espósito CC, et al. Heterologous mesenchymal stem cells successfully treat femoral pseudarthrosis in rats. J Transl Med 2012;10:51. doi:10.1186/1479-5876-10-51.

[30] Yang L, Zhu W, Cui J, Huang J, Liao F, Duan L, et al. Repairing Effect of a Nano-Artificial Bone Combined with HIF-1α Transfected Bone Marrow Mesenchymal Stem Cells for Rabbit Radial Bone Defects. J Biomater Tissue Eng 2016;6:767–74.

[31] Gimeno M, Pinczowski P, Vázquez FJ, Pérez M, Santamaría J, Arruebo M, et al. Porous orthopedic steel implant as an antibiotic eluting device: Prevention of post-surgical infection on an ovine model. Int J Pharm 2013;452:166–72. doi:10.1016/j.ijpharm.2013.04.076.

[32] Talley AD, Boller LA, Kalpakci KN, Shimko DA, Cochran DL, Guelcher SA. Injectable, compression-resistant polymer/ceramic composite bone grafts promote lateral ridge augmentation without protective mesh in a canine model. Clin Oral Implants Res 2018;29:592–602.

[33] Dai Y, Liu H, Liu B, Wang Z, Li Y, Zhou G. Porous β-Ca2SiO4 ceramic scaffolds for bone tissue engineering: In vitro and in vivo characterization. Ceram Int 2015:1–9. doi:10.1016/j.ceramint.2015.01.021.

[34] Segundo FA de S, Costa EI de S, Azevedo AS de, Araújo AL de, Silva AC de F, de Lima GG, et al. Platelet-Rich Plasma, Hydroxyapatite, and Chitosan in the Bone and Cartilaginous Regeneration of Femoral Trochlea in Rabbits: Clinical, Radiographic, and Histomorphometric Evaluations. J Healthc Eng 2018;2018.

[35] Le Guéhennec L, Layrolle P, Daculsi G. A Review of Bioceramics and Fibrin Sealant. Eur Cells Mater 2004;8:1–11. doi:10.22203/eCM.v008a01.

[36] Oryan A, Alidadi S. Reconstruction of radial bone defect in rat by calcium silicate biomaterials. Life Sci 2018;201:45–53. doi:10.1016/j.lfs.2018.03.048.

[37] Sheikh Z, Zhang YL, Tamimi F, Barralet J. Effect of processing conditions of dicalcium phosphate cements on graft resorption and bone formation. Acta Biomater 2017;53:526–35.